arXiv:1412.0787v1 [quant-ph] 2 Dec 2014

A black potential for spin less particles

Ananya Ghatak [1], Mohammad Hasan [2] and Bhabani Prasad Mandal [3]

[1,3]*Department of Physics, Banaras Hindu University, Varanasi-221005, INDIA.*
[2]*ISRO Satellite Centre (ISAC), Bangalore-560017, INDIA*

Abstract

We consider the most general non-Hermitian Hulthen potential to study the scattering of spin-less relativistic particles. The conditions for CC, SS and CPA are obtained analytically for this potential. We show that almost total absorption occurs for entire range of incidence energy for certain parameter ranges of the potential and hence term this as 'black potential'. Time reversed of the same potential shows perfect emission for the entire range of particle energy. We also present the classical analog of this potential in terms of waveguide cross section.

[1]e-mail address: gananya04@gmail.com
[2]e-mail address: mohammadhasan786@gmail.com
[3]e-mail address: bhabani.mandal@gmail.com, bhabani@bhu.ac.in

1 Introduction

Certain class of non-Hermitian systems with real energy eigenvalues has become the topic of frontier research over a decade and half because one can have fully consistent quantum theory by restoring the Hermiticity and upholding the unitary time evolution for such system in a modified Hilbert space [1]-[3]. The study of non-Hermitian system has received a huge boost in this decade when some of the predictions of such theories were experimentally observed in optics [4]-[7] and therefore such theories have found many applications in different branches of physics [8]-[12]. Non-Hermitian theories have very rich scattering properties. Various features of scattering due to non-Hermitian potential like exceptional points (EPs) [13]-[15], spectral singularity (SS) [16]-[19], invisibility [18]-[21], reciprocity [18]-[22], coherent perfect absorption (CPA) [23]-[31] and critical coupling (CC) [32]-[36] have generated huge interests during last few years due to their applicability and usefulness in the study of different optical systems. CPA or CC, the time reversal of lasing effect has become very exciting due to the discovery of anti-laser [23]-[25] which has number of applications in optical computer, radiology etc. This phenomena of perfect absorption can be observed in quantum scattering when waves interact with the surrounding medium through a complex potential distribution. The event of null transmission and reflection in the case of unidirectional incidence is named as critical coupling. The occurrence of CPA takes place when the waves incident from both directions on a potential and then interfere with one another in such a way as to perfectly cancel each other out. These two significant phenomena of total absorption can have more variety of consequences and applications in different branches of science. However CPA and CC have so far been showed for some discrete incidence energies for certain specific complex potential [37]. Recently we have been able to find certain small ranges of incidence energies for CC and CPA in a particular system [38].

The aim of this work is to construct a complex potential in such a manner that it behaves almost as a perfect absorber (or a perfect emitter) for the entire range of incidence energy. For this purpose we consider the general one dimensional Hulthen potential written as,

$$V(z) = \theta(-z)\frac{V_1}{e^{-\alpha_1 z} - Q_1} + \theta(z)\frac{V_2}{e^{\alpha_2 z} - Q_2} \; ; \tag{1}$$

which has six independent real and/or complex parameters V_1, V_2, Q_1, Q_2, α_1, α_2. $\theta(z)$ the Heaviside step function is defined as,

$$\begin{aligned} \theta(z) &= 1 \;\; \text{for} \;\; z \geq 0 \; ; \\ &= 0 \;\; \text{for} \;\; z < 0 \end{aligned} \tag{2}$$

This potential can be parametrized in many ways for PT-symmetric (as well as non PT-symmetric) non-Hermitian configurations. The left and right scattering coefficients for this complex non-Hermitian potential are calculated by solving corresponding Klein-Gordon(KG) equation to capture various characteristics in different parametric regime.

We intend to focus on the non-Hermitian configurations of this potential to study the occurrence of perfect absorption for entire range of incidence energy.

The conditions of null as well as super scattering are obtained analytically and are also demonstrated graphically. We find a region in the space of the parameters of this potential where it behaves almost[4] as a perfect absorber (or emitter) for the entire range of the incident particle energy resulting a broadband CPA. This specific potential because of its absorption properties is termed as a 'black potential'. At very low energy almost CPA is also achieved by further fine tunning the parameters within their allowed regimes. The time reversed of the same potential shows the similar behavior reversely for the entire range of the incident particle energy. The waveguide analog of this potential is also presented for classical realization. Physical dimension of the waveguide and operating frequency are calculated.

Different aspects of scattering and absorption in the Non-Hermitian potential are discussed in Sec. 2. Sec. 2.1 is devoted for low energy scattering and critical coupling. Bidirectional absorption is discussed in Sec. 2.2. Waveguide analog for this potential is demonstrated in Sec. 3. Sec. 4 is kept for conclusions and discussions. Necessary mathematical details are provided in Appendix.

2 Scattering and absorption in the Non-Hermitian Hulthen potential

The most general non-Hermitian structure of the Hulthen potential in Eq. 1 is obtained by complexifying all the parameters as,

$$V_{1,2} \to v_{1,2}e^{i\beta_{1,2}} \ ; \ \ \alpha_{1,2} \to a_{1,2}e^{i\gamma_{1,2}} \ ; \ \ Q_{1,2} \to q_{1,2}e^{i\phi_{1,2}} \ . \tag{3}$$

where v_1, v_2, a_1, a_2, q_1, q_2 are all real numbers and assumed to be positive definite for convenience and the arguments β_1, β_2, γ_1, γ_2, ϕ_1, ϕ_2 are all taken between 0 to 2π. $v_{1,2}$, $a_{1,2}$ have dimension of energy and length inverse respectively where as $q_{1,2}$, $\beta_{1,2}$, $\gamma_{1,2}$ and $\phi_{1,2}$ are dimensionless. We solve the 1-D KG equation,

$$\frac{d^2\phi(z)}{dz^2} + \Big\{\frac{[E-V(z)]^2}{c^2\hbar^2} - \frac{m^2c^2}{\hbar^2}\Big\}\phi(z) = 0 \tag{4}$$

for non-Hermitian potential in Eq. 1 with complex parameters defined in Eq. 3 for $z < 0$ and $z > 0$ by following Ref. [39]. The wave functions and their asymptotic behaviors are explicitly given in Appendix. For convenience we adopt natural unit ($\hbar = c = 1$) and chose the mass (m) of the incident particle as $1MeV$, $v_{1,2}$ and $a_{1,2}$ in MeV and z in MeV^{-1} for physical realization. MeV^{-1} can be converted in nanometer (nm) using the conversion relation $1MeV^{-1} = 1.97 \times 10^{-4}nm$ for practical purposes.

[4]R and T can not vanish rigorously over a range of continuous energy [40, 41].

The scattering amplitudes for left and right incidence are calculated by demanding the continuity of the wave functions and their derivatives at $z = 0$. The scattering amplitudes for left incident case are written in the compact form as,

$$r_l = Q_1^{2\mu_1} \frac{\Big[- F_1F_2(N_1 + N_2) + c_1F_1^{'}F_2 + c_3F_2^{'}F_1\Big]}{2MF_4F_2 + F_4F_2(N_1 + N_2) - c_2F_4^{'}F_2 - c_3F_2^{'}F_4} \equiv Q_1^{2\mu_1}\tilde{F}_{rl} \ ; \tag{5}$$

$$t_l = Q_1^{2\mu_1} \frac{\Big[2MF_1F_4 + c_1F_1^{'}F_4 - c_2F_4^{'}F_1\Big]}{2MF_4F_2 + F_4F_2(N_1 + N_2) - c_2F_4^{'}F_2 - c_3F_2^{'}F_4} \left(\frac{1}{u}\right) \equiv \frac{Q_1^{2\mu_1}}{u}\tilde{F}_{tl} \ ; \tag{6}$$

where,

$$\mu_1 = ik/\alpha_1 \ \ ; \ \ \mu_2 = ik/\alpha_2 \ \ ; \ \ k = \sqrt{E^2 - 1} \ ; \tag{7}$$

$$N_1 = \frac{Q_1\alpha_1\lambda_1}{1 - Q_1} \ ; \ N_2 = \frac{Q_2\alpha_2\lambda_2}{1 - Q_2} \ ; \tag{8}$$

$$u = \frac{Q_2^{-\mu_2}(1 - Q_2)^{\lambda_2}}{Q_1^{-\mu_1}(1 - Q_1)^{\lambda_1}} \ ; \tag{9}$$

$$\begin{aligned} c_1 &= \frac{(\mu_1 + \lambda_1)^2 - \nu_1^2}{1 + 2\mu_1}(Q_1\alpha_1) \ \ ; \ \ c_2 = \frac{(-\mu_1 + \lambda_1)^2 - \nu_1^2}{1 - 2\mu_1}(Q_1\alpha_1) \ ; \\ c_3 &= \frac{(-\mu_2 + \lambda_2)^2 - {\nu_2}^2}{1 - 2\mu_2}(Q_2\alpha_2) \ \ ; \ \ c_4 = \frac{(\mu_2 + \lambda_2)^2 - {\nu_2}^2}{1 + 2\mu_2}(Q_2\alpha_2) \ ; \end{aligned} \tag{10}$$

with

$$\lambda_1 = 1/2 + 1/2\sqrt{1 - \Big(\frac{2V_1}{\alpha_1Q_1}\Big)^2} \ \ ; \ \lambda_2 = 1/2 + 1/2\sqrt{1 - \Big(\frac{2V_2}{\alpha_2Q_2}\Big)^2} \ ; \tag{11}$$

$$\nu_1 = \sqrt{\mu_1^2 + \lambda_1^2 - \lambda_1 - \frac{2EV_1}{\alpha_1^2Q_1}} \ \ ; \ \ \nu_2 = \sqrt{\mu_2^2 + \lambda_2^2 - \lambda_2 - \frac{2EV_2}{\alpha_2^2Q_2}} \ . \tag{12}$$

The functions $\tilde{F_{rl}}$ and $\tilde{F_{tl}}$ in reflection and transmission amplitudes in Eqs. 5 and 6 contain the contributions from hyper-geometric functions (given in Eqs. 78-81 in Appendix). At the very outset we concentrate on the CC for left incidence (i.e. $T_l \equiv \mid t_l \mid^2 \rightarrow 0$ and $R_l \equiv \mid r_l \mid^2 \rightarrow 0$) by looking at the behavior of r_l and t_l for different incidence energies. We first look at the behavior of the terms $Q_1^{2\mu_1}$ in r_l and $Q_1^{2\mu_1}\frac{1}{u}$ in t_l which involve no hyper-geometric functions. $Q_1^{2\mu_1}$ is written in terms of the parameters in Eq. 3 as,

$$Q_1^{2\mu_1} = (q_1e^{i\phi_1})^{2\frac{k}{a_1}e^{i(\frac{\pi}{2} - \gamma_1)}} \ . \tag{13}$$

Using an identity

$$|(Ae^{ia})^{Be^{ib}}| = e^{B(\cos b \ln A - a \sin b)}, \ \ \text{where } A, B, a, b \text{ are all real,} \tag{14}$$

we further re-express Eq. 13 as,

$$|Q_1^{2\mu_1}| = e^{\frac{2k}{a_1}(\sin\gamma_1 \ln q_1 - \phi_1 \cos\gamma_1)} \equiv e^{\frac{2k}{a_1}\xi_1} \tag{15}$$

with

$$\xi_1 = \sin\gamma_1 \ln q_1 - \phi_1 \cos\gamma_1 \tag{16}$$

It is clear from Eq. 15 that $|Q_1^{2\mu_1}|$ can play an important role as it contributes exponentially with increasing energy. The contribution of this term be enhanced further for small a_1. As shown in Fig. 1(a) this term has huge contribution to r_l with increasing energy for smaller values of a_1. In comparison to this the behavior of $\tilde{F}_{rl}$ (for $|Q_1| < 1$) shows saturating nature with increasing energy (Fig. 1(b)). Therefore that $|Q_1^{2\mu_1}|$ is the most dominating term in r_l with increasing energy and is responsible for super or null reflectivity. The occurrence of null reflectivity depends upon the sign of the term ξ_1 in the exponential of Eq. 15. We define the critical value of the parameter γ_1 as,

$$\gamma_1^c = \tan^{-1}\frac{\phi_1}{\ln q_1} \tag{17}$$

For $\gamma_1 > \gamma_1^c$, ξ_1 is positive and $R_l = |r_l|^2$ is going to very high values with increasing energy (Fig. 1(c)).

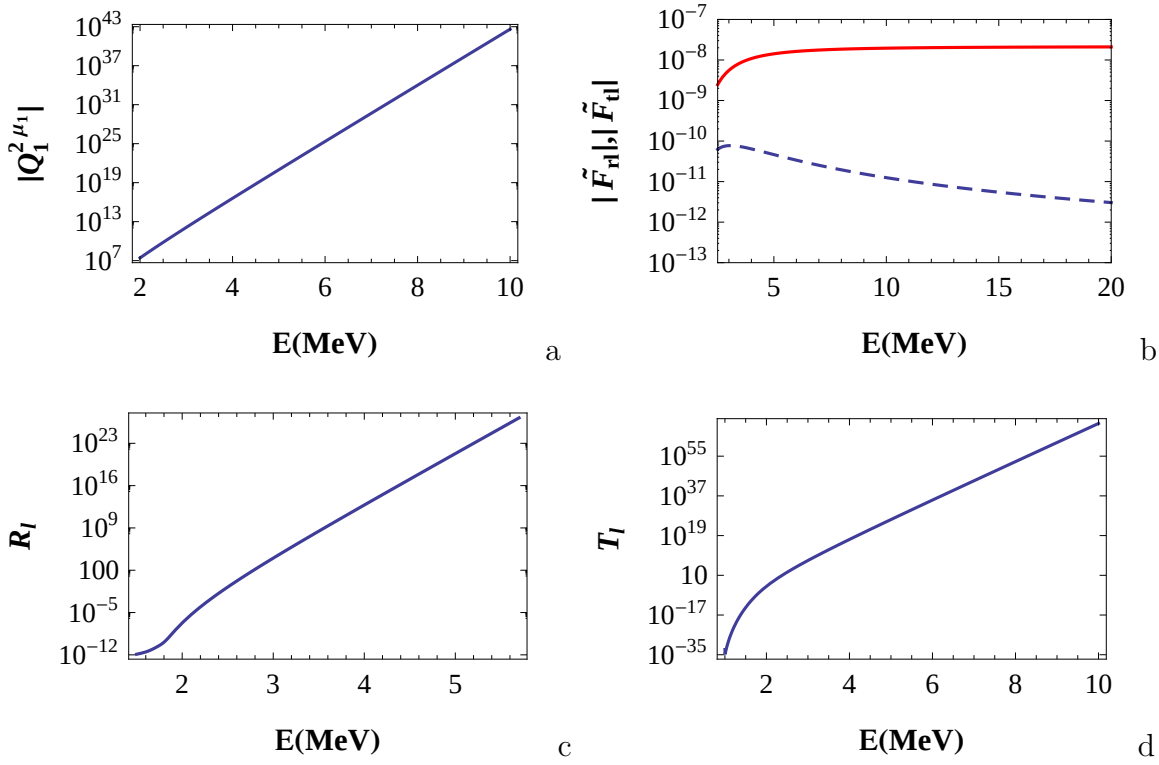

Fig. 1: The behavior of $|Q_1^{2\mu_1}|$ in 1(a) and $\left|\tilde{F}_{rl}\right|$ (dotted line), $\left|\tilde{F}_{tl}\right|$ (solid line) in 1(b) are shown for the choice of the parameters as $q_1 = q_2 = 0.4, v_1 = v_2 = 1MeV, a_1 = a_2 = 0.1MeV, \phi_1 = \phi_2 = 1.3, \gamma_1 = \gamma_2 = 2.5, \beta_1 = \beta_2 = 0.2$, leading $\gamma_1 > \gamma_1^c$. R_l and T_l with the same set of parameters are plotted in 1 (c) and 1 (d) respectively.

On the other hand for $\gamma_1 < \gamma_1^c$ we have almost null reflectivity ($R_l \sim 10^{-24}$ and less) for the entire range of energy (Fig. 2(a)) except at very low energy. The scattering at very low energy is different in nature and has been dealt with separately in the next section.

Similarly for transmission amplitude t_l the dominant factor (hyper-geometric function independent part) is written using the expression of u in Eq. 8 as,

$$Q_1^{2\mu_1}\frac{1}{u} = Q_1^{\mu_1}Q_2^{\mu_2}\frac{(1-Q_1)^{\lambda_1}}{(1-Q_2)^{\lambda_2}} \equiv f_1 f_2 \tag{18}$$

(where $\mu_{1,2}$ and $\lambda_{1,2}$ are given in Eqs. 7, 11) with

$$f_1 = Q_1^{\mu_1}Q_2^{\mu_2} \;\; ; \;\; f_2 = \frac{(1-Q_1)^{\lambda_1}}{(1-Q_2)^{\lambda_2}} \tag{19}$$

so that

$$|Q_1^{2\mu_1}\frac{1}{u}| = |f_1||f_2| \tag{20}$$

$|f_2|$ depends only on the potential parameters and independent of k. The energy dependence of $|Q_1^{2\mu_1}\frac{1}{u}|$ is only through $|f_1|$, which is re-expressed (again by using the identity in Eq. 14) as,

$$|f_1| = e^{k[\frac{1}{a_1}(\sin\gamma_1 \ln q_1 - \phi_1\cos\gamma_1)+\frac{1}{a_2}(\sin\gamma_2 \ln q_2 - \phi_2\cos\gamma_2)]} \equiv e^{k[\frac{\xi_1}{a_1}+\frac{\xi_2}{a_2}]} \tag{21}$$

The variation of $\tilde{F}_{tl}$ in Eq. 6 is not dominating as shown in the Fig. 1(b). The behavior of $T_l = |t_l|^2$ depends on the overall sign of the exponential in $|f_1|$. We already have the reflection-less condition for $\xi_1 < 0$, so we discuss the possible conditions of CC in high energy ($a_{1,2} < k$) range as follows.

Case 1: $\boldsymbol{\xi_2 < 0}$; $\boldsymbol{\xi_1 < 0}$; $\mathbf{a_{1,2} < k}$;

Since ξ_1, ξ_2 both are negative we have total absorption with increasing energy of left incident particle. The critical values of $\gamma_{1,2}$ are written in terms of the other parameters as,

$$\gamma_{1,2}^c = \tan^{-1}\frac{\phi_{1,2}}{\ln q_{1,2}}; \tag{22}$$

Thus we have total absorption for entire range of both left and right incident waves for $\gamma_{1,2} < \gamma_{1,2}^c$. For symmetric Hulthen potential (i.e. when $\alpha_1 = \alpha_2, Q_1 = Q_2$ and $V_1 = V_2$) if we consider a special case of $q_{1,2} = 1$, then CC occurs when γ_1 lies between $0 \to \pi/2$ or $\frac{3\pi}{2} \to 2\pi$ with any arbitrary value of ϕ_1 between 0 to 2π.

Case 2: $\xi_2 > 0$; $\xi_1 < 0$; $a_{1,2} < k$;

The condition of critical coupling is achieved if and only if $\left(-\frac{|\xi_1|}{a_1} + \frac{|\xi_2|}{a_2}\right) < 0$ which suggests,

$$\begin{aligned} |\,\xi_1\,| &> \frac{a_1}{a_2}\,|\,\xi_2\,| \quad \text{i.e. ,} \\ \phi_1 \cos\gamma_1 + \frac{a_1}{a_2}\phi_2 \cos\gamma_2 &> \frac{a_1}{a_2}\sin\gamma_2 \ln q_2 + \sin\gamma_1 \ln q_1 \end{aligned} \tag{23}$$

Eq. 23 is realized in a simpler way if we take a specific choice of some of the parameters as $q_1 = q_2, \phi_1 = \phi_2$ and $a_1 = a_2$. For this choice we get a upper bound for $(\gamma_1 + \gamma_2)$ from Eq. 23 to have CC as,

$$(\gamma_1 + \gamma_2)^c = 2\tan^{-1}(\phi_1/\ln q_1)\,. \tag{24}$$

From the above two cases we note that when $\gamma_{1,2} > \gamma_{1,2}^c$ [or $(\gamma_1 + \gamma_2) > (\gamma_1 + \gamma_2)^c$] we get resonances in transmissivity for all ranges of incidence energy. Fig. 1(d) shows the very high values of $T_l = |t_l|^2$ as incident energy increases. On the other hand almost null transmissivity ($T_l \sim 10^{-36}$) for left incidence (Fig. 2(b)) occurs for almost all the values of incidence energy (except low energy) when $\gamma_{1,2} < \gamma_{1,2}^c$ or $(\gamma_1 + \gamma_2) < (\gamma_1 + \gamma_2)^c$.

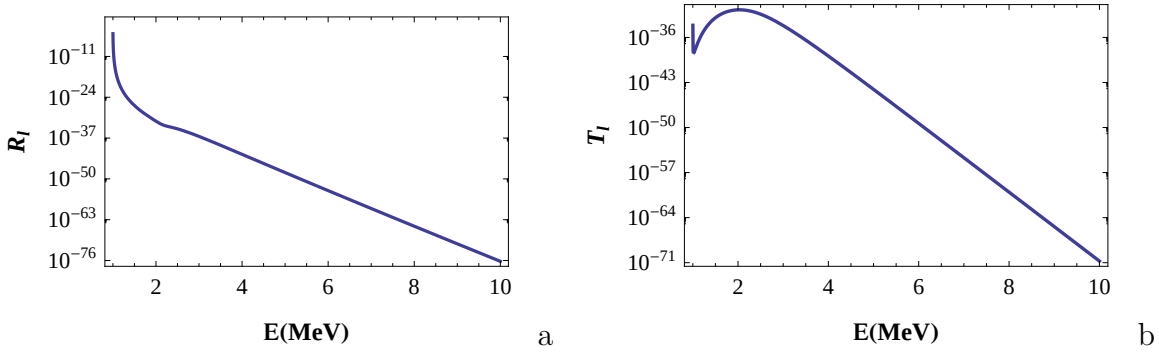

Fig. 2: R_l (in 2(a)) and T_l (in 2(b)) are plotted with incidence energy by changing $\phi_{1,2}(= 0.3)$ and keeping other parameters same as Fig.1 for $\gamma_1 < \gamma_1^c$. Almost null transmissivity and reflectivity for left incidence are seen ($T_l \sim 10^{-36}$ or less and $R_l \sim 10^{-24}$ or less) at all energies except at low incidence energy.

Thus we have almost null scattering for unidirectional incidence occurs for almost all the values of incidence energy (except at low energy) subjected to the conditions $a_{1,2} < k$, $\gamma_{1,2} < \gamma_{1,2}^c$ or $(\gamma_1 + \gamma_2) < (\gamma_1 + \gamma_2)^c$ when both the scattering amplitudes R_l and T_l are almost vanishing (as shown in Fig. 2). However when $\gamma_{1,2} > \gamma_{1,2}^c$ [or $(\gamma_1+\gamma_2) > (\gamma_1+\gamma_2)^c$] we get resonances in scattering amplitudes for all ranges of incidence energy (Fig. 1(c,d)). Surprisingly this situation is different from the time reversed case of CC. The same characteristics are also seen for the right incidence case. Real and imaginary parts of the symmetric Hulthen potential is plotted in Fig. 3(a) keeping the

parameters same as in Fig. 2. The imaginary part of the potential (dashed curve in Fig. 3(a)) is responsible for the unidirectional total absorption of almost all the incident energies except the low energy. Fig. 3(b,c,d) are relevant to the discussion of low energy scattering in the next section.

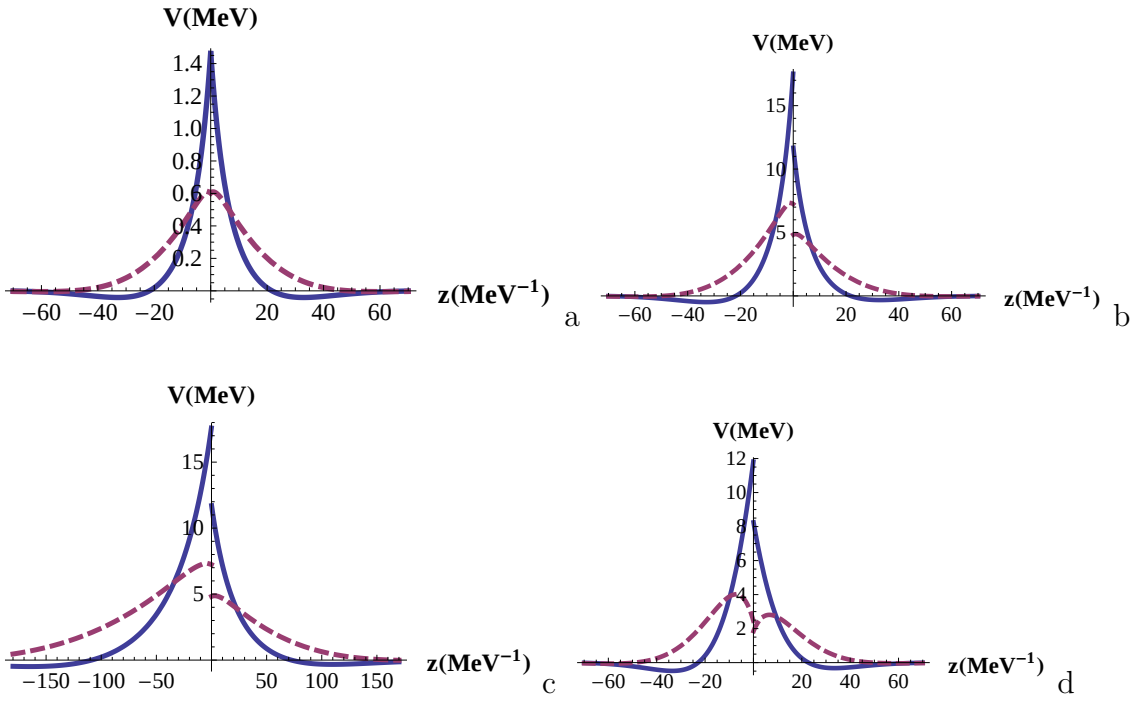

Fig. 3: The real part (solid lines) and imaginary part (dashed lines) of symmetric (3(a)) as well as asymmetric (3(b,c,d)) non-Hermitian Hulthen potential are plotted in the parametric regime of CPA. Fig 3(a) shows the symmetric potential in the same parametric regime of Fig. 2. Fig 3(b) is plotted by changing the values of $v_1(= 12MeV)$ *and* $v_2(= 8MeV)$*. In Fig 3(c)* $q_{1,2}$ *are changed to* $q_1 = 0.01$ *and* $q_2 = 0.06$*. Fig 3(d) is for different* $a_1(= 0.02MeV^{-1})$ *and* $a_2(= 0.03MeV^{-1})$*.*

2.1 Low energy scattering

In the low energy region the phenomena of total absorption may not occur even though the condition of $\gamma_{1,2} < \gamma_{1,2}^c$ [or $(\gamma_1 + \gamma_2) < (\gamma_1 + \gamma_2)^c$] is satisfied. This is also clear from the Figs. 1 and 2. At low energy region, $k \simeq a_{1,2}$ and therefore the contributions of the exponential terms in Eqs. 15 and 21 are not dominating. However we obtain perfect absorption even at low energy region by tunning the parameters further within their ranges and by studying the behavior of the other terms in r_l and t_l. In the following subsections we first study the terms with hyper-geometric functions to see if they have important impact on deciding the extreme behavior of r_l and t_l in this region. We further study the impact of the energy independent term f_2 present in t_l in this low energy region.

2.1.1 The terms $\tilde{F_{tl}}$ and $\tilde{F_{rl}}$

Each hyper-geometric functions (see Eq. 78 -81 for the explicit expressions) in $\tilde{F_{tl}}$ and $\tilde{F_{rl}}$ converge with respect to energy to an asymptotic value for $|Q_{1,2}| = q_{1,2} < 1$. But in the low energy region they have variety of behaviors depending on the different values of the parameters. The terms $\lambda_{1,2}$ and $\nu_{1,2}$ (given in Eqs. 11 and 12) in all the hyper-geometric functions have the following limiting cases in the low energy region when k is comparable to $a_{1,2}$,

$$\text{(I)} \quad \text{for } \left|\frac{V_{1,2}}{\alpha_{1,2}Q_{1,2}}\right| >> 1 \ : \tag{25}$$

we can write from Eqs. 11 and 12,

$$|\lambda_{1,2}| \approx \left|\frac{V_{1,2}}{\alpha_{1,2}Q_{1,2}}\right| \ ; \ |\nu_{1,2}| \approx \left|\frac{V_{1,2}}{\alpha_{1,2}Q_{1,2}}\right| \ , \tag{26}$$

as in this low energy region $|\mu_{1,2}| = |\frac{ik}{\alpha_{1,2}}| \sim 1$ and we see from Eq. 12 that $\left|\mu_{1,2}^2 - \lambda_{1,2} - \frac{2EV_{1,2}}{\alpha_{1,2}^2 q_{1,2}}\right| \sim |\lambda_{1,2}|$ and $|\lambda_{1,2}^2| >> |\lambda_{1,2}|$.

$$\text{(II)} \quad \text{for } \left|\frac{V_{1,2}}{\alpha_{1,2}Q_{1,2}}\right| << 1 \ : \tag{27}$$

from Eqs. 11 and 12 we see that

$$\lambda_{1,2} \approx 1 \ \ ; \ \ \nu_{1,2} \approx \sqrt{\mu_{1,2}^2 - \frac{2V_{1,2}E}{\alpha_{1,2}^2 Q_{1,2}}} \approx \mu_{1,2} \ . \tag{28}$$

Now for simplicity we consider a symmetric complex Hulthen potential ($\alpha_1 = \alpha_2, Q_1 = Q_2, V_1 = V_2$) for case-I. Putting the values of λ_1, ν_1 from Eq. (26) in the Eqs. (8) and (10) we obtain,

$$N_1 = \frac{iV_1}{1-Q_1} = N_2 \ ; \ c_1 = c_4 = \frac{2i\mu_1 V_1}{1+2\mu_1} = -c_2 = -c_3 \ . \tag{29}$$

For this symmetric case we see from Eqs. (79) and (81) that $F_2 = F_4$ and $F_2^{'} = F_4^{'}$, therefore in this limit $\tilde{F_{rl}}$ is written by using Eq. (29) as,

$$\left|\tilde{F_{rl}}\right| = \frac{\left|-F_1F_4(\frac{2V_1}{1-Q_1}) + (\frac{2\mu_1V_1}{1+2\mu_1})F_1^{'}F_4 - (\frac{2\mu_1V_1}{1+2\mu_1})F_4^{'}F_1\right|}{\left|2Me^{\frac{-i\pi}{2}}F_4^2 + F_4^2(\frac{2V_1}{1-Q_1}) + (\frac{2\mu_1V_1}{1+2\mu_1})F_4^{'}F_4 + (\frac{2\mu_1V_1}{1+2\mu_1})F_4^{'}F_4\right|} \tag{30}$$

where $F_{i=1,2,3,4}$ (and $F^{'}{}_{i=1,2,3,4}$) are given in Appendix. Further in this limiting case, it can be shown by using the properties of hyper-geometric function [42] that $|F_1| \approx |F_4|$ and $|F_1^{'}| \approx |F_4^{'}|$ as $|\nu_1|$ and $|\lambda_1|$ are being much larger comparable to $|\mu_1|$ in low energy region. Hence from Eq. 30 it is easily seen that the denumerator is always larger than the numerator. Therefore for convenient values of v_1 and/or a_1, the reflection coefficient

vanishes as $\left|\tilde{F_{rl}}\right| \to 0$ in the low energy region. These have been demonstrated in Figs. 4(a, b).

Similarly for transmission coefficient in this energy region and for a symmetric potential case the term $\tilde{F_{tl}}$ is written as,

$$\left|\tilde{F_{tl}}\right| = \frac{\left|2Me^{\frac{-i\pi}{2}}F_1F_4 + (\frac{2\mu_1V_1}{1+2\mu_1})F_1'F_4 + (\frac{2\mu_1V_1}{1+2\mu_1})F_4'F_1\right|}{\left|2Me^{\frac{-i\pi}{2}}F_4^2 + F_4^2(\frac{2V_1}{1-Q_1}) + (\frac{2\mu_1V_1}{1+2\mu_1})F_4'F_4 + (\frac{2\mu_1V_1}{1+2\mu_1})F_4'F_4\right|} \tag{31}$$

From this equation we see that $\left|\tilde{F_{tl}}\right|$ goes to zero even faster than $\left|\tilde{F_{rl}}\right|$ resulting $T_l \to 0$ in the low energy region (Figs. 4(a, b)). On the other hand from case II, we do not get such parametric regime for which perfect absorption is achieved. Thus in this low energy region these hyper-geometric functions play important roles over the previously discussed exponential terms and lead to total absorption. We further study the total absorptivity $(A_l = 1 - R_l - T_l)$ for left incidence with different values of v_1 following the above discussion. A_l has been plotted in Figs. 4(c) and 4(d) for two different values of v_1 to show the total absorption at low energy.

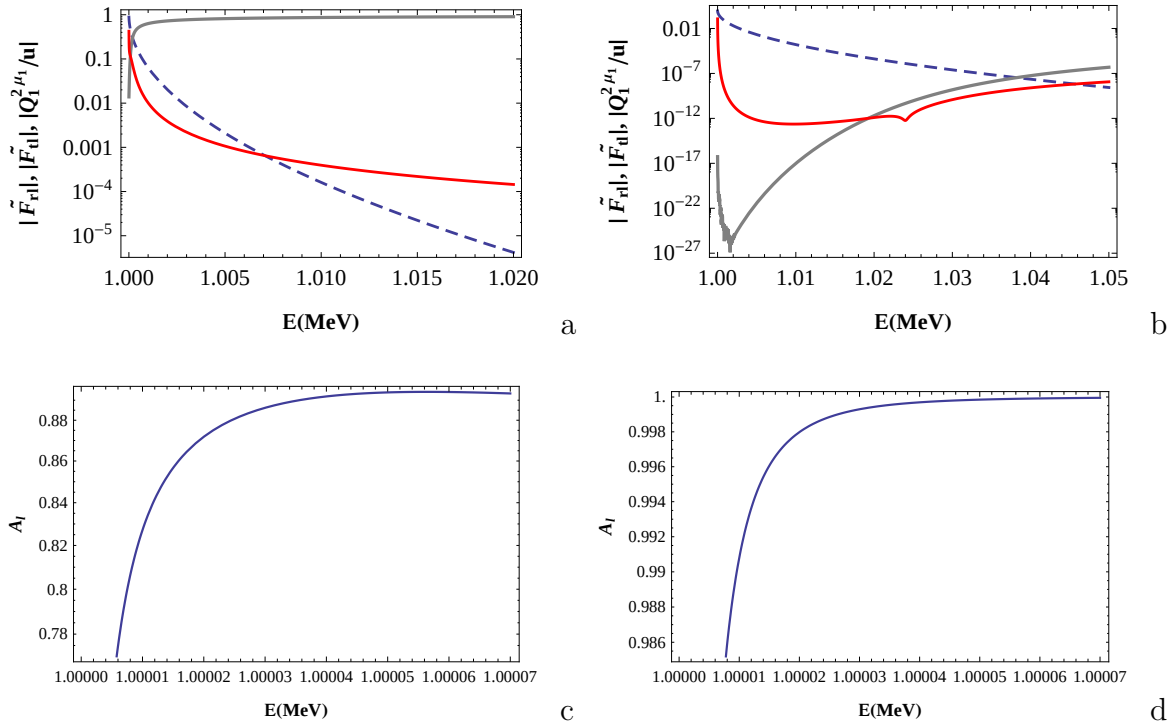

Fig. 4: 4 (a) and 4 (b) are showing the natures $\left|\tilde{F_{rl}}\right|$ *(solid red line) ,* $\left|\tilde{F_{tl}}\right|$ *(solid gray line) and* $\left|Q_1^{2\mu_1}\frac{1}{u}\right|$ *(dashed line) in low energy region for two different values of* $v_{1,2}$*,* $v_{1,2} = .0001MeV$ *and* $v_{1,2} = .02MeV$ *respectively and* $a_{1,2} = .01MeV^{-1}$*. 4 (c) (with* $v_{1,2} = .0001MeV$*) and 4 (d) (with* $v_{1,2} = .02MeV$*) show the total absorption in low energy ranges.*

The real and imaginary parts of the non-Hermitian asymmetric Hulthen potentials are plotted in Fig. 3(b,c,d) with different parameters for which almost perfect absorption occurs at high energy as well as in the low energy limit (subjected to the condition in Eq. 25). Fig. 3 also clarifies the contributions of the parameters $(v_{1,2}, a_{1,2}, q_{1,2})$ to the real and imaginary parts of the potential.

2.1.2 Effect of f_2 term

Now we show that even the energy independent term f_2 plays certain role in deciding total absorption at low energy. The expression of f_2 in Eq. 19 is rewritten as,

$$f_2 = \frac{\left(\sqrt{1-Q_1}\right)^{2\lambda_1}}{\left(\sqrt{1-Q_2}\right)^{2\lambda_2}} = \frac{(\rho_1 e^{i\tau_1})^{2\lambda_1}}{(\rho_2 e^{i\tau_2})^{2\lambda_2}} \tag{32}$$

where

$$\rho_{1,2} = (1 + q_{1,2}^2 - 2q_{1,2}\cos\phi_{1,2})^{\frac{1}{4}} \; ; \quad \tau_{1,2} = \frac{1}{2}\tan^{-1}\Big[\frac{q_{1,2}\sin\phi_{1,2}}{q_{1,2}\cos\phi_{1,2} - 1}\Big] \tag{33}$$

We have already seen the criterion for total absorption for low energy region in the previous section as $\left|\frac{V_{1,2}}{\alpha_{1,2}Q_{1,2}}\right| >> 1$. From Eq. 26 the terms λ_1 and λ_2 are rewritten for the parameters given in Eq. 3 as,

$$\lambda_{1,2} = \left(\frac{v_{1,2}}{a_{1,2}q_{1,2}}\right) e^{i(\frac{\pi}{2}+\delta_{1,2})} \equiv l_{1,2} e^{i(\frac{\pi}{2}+\delta_{1,2})} \;\; ; \text{ with } \delta_{1,2} = \beta_{1,2} - \gamma_{1,2} - \phi_{1,2} \tag{34}$$

where $l_{1,2} = \frac{v_{1,2}}{a_{1,2}q_{1,2}}$. Using the identity in Eq. 14 we write Eq. 32 after a small trigonometric simplification as,

$$|f_2| = \frac{e^{-2\lambda_a[\sin\delta_1 \ln\rho_1 + \tau_1\cos\delta_1]}}{e^{-2\lambda_b[\sin\delta_2 \ln\rho_2 + \tau_2\cos\delta_2]}} \equiv e^{\Gamma} \tag{35}$$

where

$$\Gamma = -2\lambda_a[\sin\delta_1 \ln\rho_1 + \tau_1\cos\delta_1] + 2\lambda_b[\sin\delta_2 \ln\rho_2 + \tau_2\cos\delta_2] \tag{36}$$

$l_{1,2}$ are large for the conditions of CC at low incidence energy. Thus f_2 contributes substantially depending on the value of Γ. The sign of Γ will decide whether the transmissivity will be zero or diverging in these low energy regions. However f_2 has no role in case of symmetric Hulthen potential for which $\Gamma = 0$.

2.2 Bidirectional perfect absorption

We have discussed so far about the situation of total absorption when particles are coming only from one direction. Now we wish to explore the possibility of total absorption for

all energies when particles are coming from both the directions. We first re-express the scattering amplitudes in Eqs. 70-73 in the Appendix by introducing G_i $(i = 1, 2, 3, 4)$ as,

$$r_l = Q_1^{2\mu_1}\frac{G_1}{D}\ ;\ t_l = \frac{Q_1^{2\mu_1}}{u}\frac{G_2}{D} \tag{37}$$

$$r_r = Q_2^{2\mu_2}\frac{G_3}{D}\ ;\ t_r = Q_2^{2\mu_2}u\frac{G_4}{D} \tag{38}$$

D is defined in the Eq. 74 in appendix. For CPA the determinant of scattering matrix should vanish, i.e. $\mid t_l t_r - r_l r_r \mid = 0$. Using Eqs. 37 and 38 the condition for CPA is expressed as,

$$Q_1^{2\mu_1}Q_2^{2\mu_2}(G_1G_2 - G_3G_4) = 0 \tag{39}$$

The above condition is satisfied if $G_1G_2 = G_3G_4$, which describes the occurrence of coherent perfect absorption at discrete incidence energies of the waves coming from both the directions. The other conditions of total absorption in Eq. 39 show critical coupling for which $Q_1^{2\mu_1} = 0$ (CC for left incidence) or $Q_2^{2\mu_2} = 0$ (CC for right incidence). However it is possible to find a parametric regime of the potential for which $Q_1^{2\mu_1}, Q_2^{2\mu_2}$ are extremely small for almost all incident energy leading to broadband CPA for bidirectional incidence. The values of the parameters of the potential to satisfy the criteria $Q_1^{2\mu_1} \simeq 0$ and $Q_2^{2\mu_2} \simeq 0$ are already elaborated in the previous sections. Thus we have possible parametric regions for which the non-Hermitian Hulthen potential (in Eq. 1) with its real and imaginary parts behaves as a 'black potential' for unidirectional as well as bidirectional incidence. We demonstrate again a non-Hermitian asymmetric Hulthen potential in Fig. 5(a) to show the almost vanishing scattering coefficients (Fig. 5(b, c, d)) for bidirectional incidence.

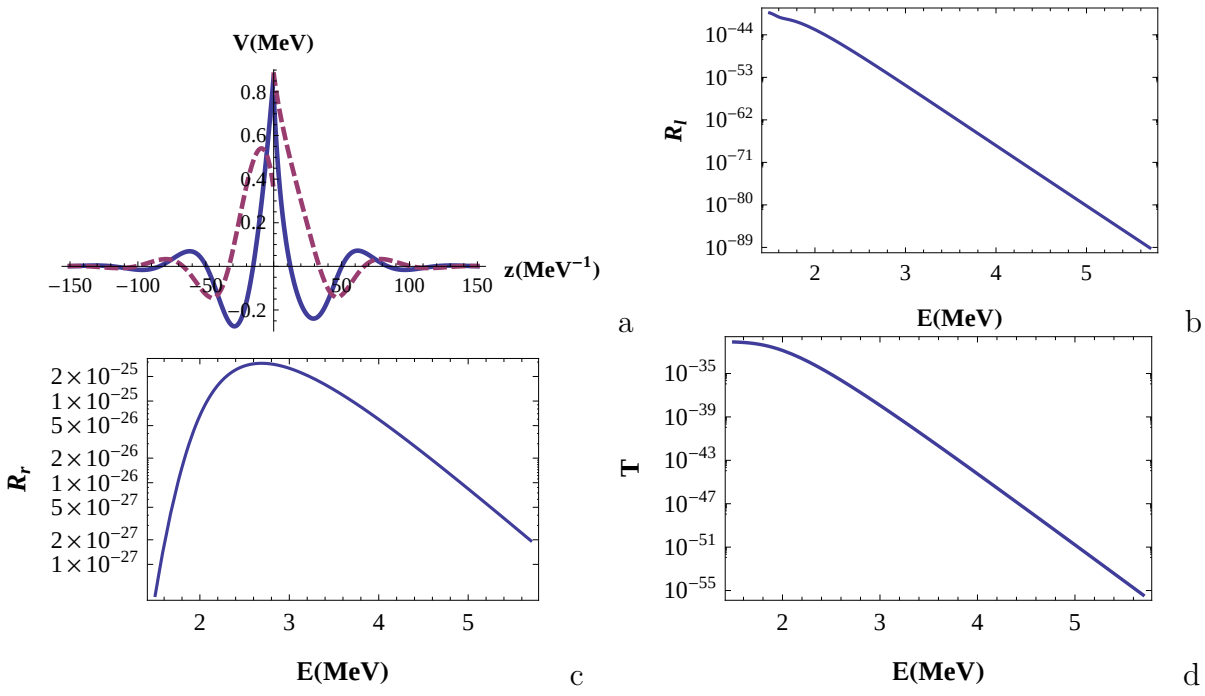

Fig. 5: Asymmetric Hulthen potential is shown in (a) ($q_1 = 0.2, q_2 = 0.4, v_1 = v_2 = 1MeV, a_1 = a_2 = 0.1MeV, \phi_1 = 1.8, \phi_2 = 1.0, \gamma_1 = \gamma_2 = 2.0, \beta_1 = \beta_2 = 0.2$,) which leads to CPA, the critical values of $\gamma_{1,2}$ are $\gamma_1^c = 2.3$ and $\gamma_2^c = 2.04$. The behaviors of scattering coefficients R_l, R_r and $T(= T_l = T_r)$ are shown in Figs. (b,c,d) which satisfy bidirectional null scattering.

This potential absorbs the energies of relativistic particles even in the ultrahigh range. Similarly all the different shapes of the potential in Fig. 3 also lie into the parametric regime of broadband CPA. The absorption rate increases with incidence energy which is an astonishing result for this potential.

To explain this result we wish to put light on three dimensional scattering by an object where the total scattering cross section σ_{tot} is the summation of total elastic scattering cross section σ_{el} and the total cross section σ_{abs} due to absorption plus inelastic scattering [43]. A perfect absorber is an object for which,

$$\sigma_{el} \approx \sigma_{abs} \approx A_{tot} \ , \quad \text{so that} \quad \sigma_{tot} \approx 2A_{tot} \tag{40}$$

where A_{tot} is the cross-sectional area of the object. In Ref. [43] the perfect absorption is discussed for non-relativistic case by Eikonal approximation ($V << E$). Following the same discussion, the scattering cross-sections for KG equation (in natural unit with $m = 1$) for a complex potential $V(r) = V_R(r) \pm iV_I(r)$ (where $r = r(x, y, z)$) is written as,

$$\sigma_{el} \approx \int_{-\infty}^{+\infty}\int_{-\infty}^{+\infty}\left\{1 + e^{2\theta} - 2\cos\left[\frac{1}{2k}\int_{-\infty}^{+\infty}({V_R}^2 - {V_I}^2)dz - (1 + \frac{1}{2k^2})\int_{-\infty}^{+\infty}V_R dz\right]e^{\theta}\right\}dxdy; \tag{41}$$

and

$$\sigma_{abs} \approx \int_{-\infty}^{+\infty}\int_{-\infty}^{+\infty}\left(1 - e^{2\theta}\right)dxdy \tag{42}$$

where

$$\theta = \mp\frac{2}{k}\int_{-\infty}^{+\infty}V_R V_I dz \pm 2(1 + \frac{1}{2k^2})\int_{-\infty}^{+\infty}V_I dz \text{ with } k = \sqrt{E^2 - 1} \tag{43}$$

For a step like potential as in our case we define quantities θ_I, θ_R as,

$$\begin{aligned}\theta_I \equiv \int_{-\infty}^{+\infty}V_I(x, y, z)dz &= \int_{-\infty}^{0}V_I^-(x, y, z)dz + \int_{0}^{+\infty}V_I^+(x, y, z)dz \ ; \\ \theta_R \equiv \int_{-\infty}^{+\infty}V_R(x, y, z)dz &= \int_{-\infty}^{0}V_R^-(x, y, z)dz + \int_{0}^{+\infty}V_R^+(x, y, z)dz \ .\end{aligned} \tag{44}$$

We apply this approach to the Hulthen potential in Eq. 1. The imaginary parts of this complexified potential for $z < 0$ and $z > 0$ are written in terms of the parameters in Eq. 3 as,

$$V_I^-(r) = \frac{e^{a_1 r\cos\gamma_1}v_1\left\{e^{a_1 r\cos\gamma_1}q_1\sin\phi_1 + \sin(a_1 r\sin\gamma_1)\right\}}{1 + q_1^2 e^{2a_1 r\cos\gamma_1} - 2q_1 e^{a_1 r\cos\gamma_1}\cos(\phi_1 + a_1 r\sin\gamma_1)}$$

$$V_I^+(r) = \frac{e^{-a_2 r\cos\gamma_2} v_2 \Big\{ e^{-a_2 r\cos\gamma_2} q_2 \sin\phi_2 - \sin(a_2 r\sin\gamma_2)\Big\}}{1 + q_2^2 e^{-2a_2 r\cos\gamma_2} - 2q_2 e^{-a_2 r\cos\gamma_2}\cos(\phi_2 - a_2 r\sin\gamma_2)} \tag{45}$$

Now there are many possibilities for $\sigma_{el} \approx \sigma_{abs}$. However we are only interested in the case of higher energy ranges ($k >> 1$) for which the integration in the expression θ in Eq. 43 is reduced to ,

$$\theta_0 \equiv \lim_{k\to\infty} \theta = \pm 2\int_{-\infty}^{+\infty} V_I dz \equiv \pm 2\theta_I \tag{46}$$

Therefore at very high energy range the elastic and inelastic scattering cross-sections are independent of incidence energy and are written as,

$$\sigma_{el} \approx \int_{-\infty}^{+\infty}\int_{-\infty}^{+\infty} \left(1 + e^{2\theta_0} - 2\cos(\theta_R)e^{\theta_0}\right) dxdy; \tag{47}$$

$$\sigma_{abs} \approx \int_{-\infty}^{+\infty}\int_{-\infty}^{+\infty} \left(1 - e^{2\theta_0}\right) dxdy \tag{48}$$

The expressions in Eqs. 47 and 48 show that at very higher energy regions the scattering cross-sections are getting saturated (i.e. depend on the potential parameters only). For $\theta_0 \to 0$, $\sigma_{abs} \to 0$ explains absorption less scattering due to a real potential. But $\theta_0 \to -\infty$ is also a possible case even though $V_I << E$ and the exponentials become negligibly small compared to unity for all trajectories x, y that pass through the object. In this case $\sigma_{el} \approx \sigma_{abs} \approx A_{tot}$ which defines a total absorptivity for the higher energy range. This justifies our result, saturation of absorptivity towards unity for higher energy range.

3 Waveguide analog of non-Hermitian Hulthen potential

Waveguide analogy [44] of a quantum mechanical potential is very useful to study the problem in classical regime. In this section we prescribe the cross-sectional view of the waveguide which is analogous to this relativistic non-Hermitian Hulthen potential. We start from the KG equation for a free particle,

$$\frac{d^2\phi(z)}{dz^2} + \Big\{\frac{E^2}{c^2\hbar^2} - \frac{m^2c^2}{\hbar^2}\Big\}\phi(z) \equiv \frac{d^2\phi(z)}{dz^2} + k_g^2\phi(z) = 0 \tag{49}$$

with the quantum mechanical propagation constant k_g which is written in terms of de-Broglie wavelength as,

$$k_g = \frac{2\pi}{\lambda_E}\ , \text{ where } \lambda_E = \frac{2\pi\hbar c}{\sqrt{E^2 - m^2c^4}} \tag{50}$$

The propagation constant of a waveguide is a function of the geometrical structure of the waveguide, its analogy with the quantum mechanical propagation constant offers a physical insight of the mathematical description of quantum scattering through a potential.

To understand further in a clear way we draw the geometrical view of a waveguide which is analogous to a general step potential $U(z)$ [Fig. 6(a)],

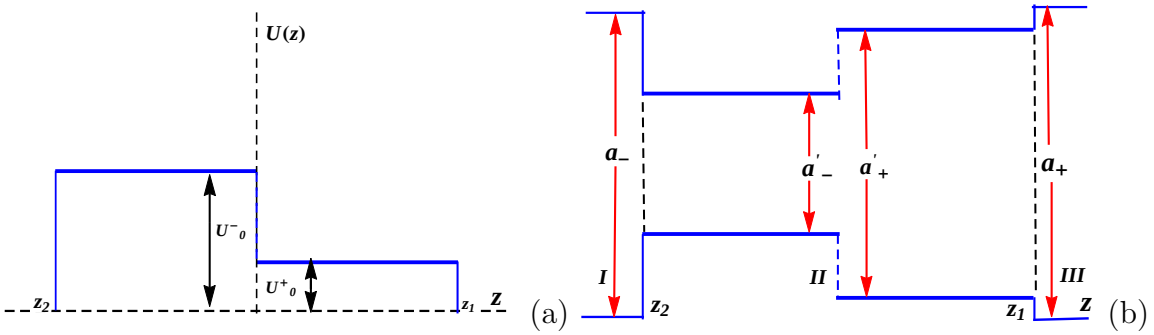

Fig. 6: The figure in right (Fig. 6(b)) demonstrates the geometrical view of a waveguide which is analogous to the general step potential shown in the left (Fig. 6(a)). Cross-sectional length of the waveguide is plotted vertically whereas $a_{\pm}(z)$, the cross-sectional distribution is plotted horizontally.

Eq. 49 is now compared to an electromagnetic wave equation [5],

$$\frac{d^2H_z}{dz^2} + k_{wg}^2 H_z = 0, \quad \text{with} \quad k_{wg} = \frac{2\pi}{\lambda}\left[1 - (\frac{\lambda}{2a_{\pm}})^2\right]^{1/2}; \tag{51}$$

for the waveguide in the region I and III of Fig. 6(b). $a_{\mp}$ are the cross-sectional lengths of the waveguide in the region I and III as depicted in Fig. 6(b). The waveguide has a cutoff wavelength $\lambda_c = 2a_{\mp}$ for the incoming waves from region I and region III respectively. By the analogy between k_g and the electromagnetic propagation constant k_{wg} we write,

$$\frac{2\pi}{\lambda_E} \propto \frac{2\pi}{\lambda}\left[1 - (\frac{\lambda}{2a_{\pm}})^2\right]^{1/2} = \frac{2\pi s}{\lambda}\left[1 - (\frac{\lambda}{2a_{\pm}})^2\right]^{1/2}, \; ; \tag{52}$$

where s is the constant of proportionality between the two propagation constants. Now for $U(z) \neq 0$ the quantum mechanical propagation constant (k_{gs}) for scattering of spin less particle due to the general step potential is calculated using the KG-equation in Eq. 4 as,

$$\begin{aligned} k_{gs} &= \left[\frac{\{E - U(z)\}^2}{c^2\hbar^2} - \frac{m^2c^2}{\hbar^2}\right]^{1/2} = 2\pi\left[\frac{E^2 - m^2c^4}{4\pi^2\hbar^2c^2}\left(1 - \frac{2EU(z) - U^2(z)}{E^2 - m^2c^4}\right)\right]^{1/2} \\ &= \frac{2\pi}{\lambda_E}\left[1 - \frac{2EU(z) - U^2(z)}{E^2 - m^2c^4}\right]^{1/2} \end{aligned} \tag{53}$$

[5]For mathematical simplicity we select the TE_{10} mode of the plane electromagnetic wave [44] whose electric and magnetic field components are oriented in a such a way that $E_x = H_y = E_z = 0$. The time-independent electromagnetic wave equation for this TE_{10} wave propagation through a waveguide is written in Eq. 51 for the region I and III of Fig. 6(b).

So the analogy between KG-equation for scattering due to the general step potential and the electromagnetic-wave equation for $\lambda < 2a'_{\pm}$ (where $a'_{\pm}$ are the cross-sectional lengths of the waveguide corresponds to the peaks of the potential $U(z)$ (i.e. $U_0^{\pm}$)) in the region II of the Fig. 6 is written as,

$$\frac{2\pi}{\lambda_E}\left[1-\frac{U(z)(2E-U(z))}{E^2-m^2c^4}\right]^{1/2}=\frac{2\pi s}{\lambda}\left[1-(\frac{\lambda}{2a_{\pm}(z)})^2\right]^{1/2} \tag{54}$$

Here $a_{\pm}(z)$ is the cross sectional distribution of the waveguide along z-direction for $z>0$ and $z<0$ respectively in region II (depicted in Fig. 6(b)). Note $a_{\pm}(z<z_2)=a_+$ and $a_{\pm}(z>z_1)=a_-$. We can see from Fig. 6(b) (as $U_0^- > U_0^+$) that the relation between a'_+ and a'_- can be written as,

$$a'_+ = a'_- + 2\left(U_0^- - U_0^+\right) \quad \text{with} \quad a'_- > 0. \tag{55}$$

Now by dividing Eq. (54) by Eq. (52) and squaring we get,

$$\frac{E^2-m^2c^4}{U(z)(2E-U(z))}=\frac{(\frac{2a_{\pm}}{\lambda})^2-1}{(\frac{a_{\pm}}{a_{\pm}(z)})^2-1} \tag{56}$$

The step potential in Fig. 6(a) can be written as $U^{\pm}(z)=U_0^{\pm}g(z)$, where $g(z)=0$ for $z>z_1$ and $z<z_2$ and $g(z)=(\theta(-z)+\theta(z))$ for $z_2\le z\le z_1$ (where $\theta(\pm z)$ is defined in Eq. 2). Now to calculate waveguide cross-section corresponding to this potential we consider the limit, incident particle energy $E\to U_0^{\pm}$ which is equivalent to $\lambda\to 2a'_{\pm}$ for case of waveguide. Putting this limiting condition in Eq. (56) we get the waveguide cross-sections as a function of z as,

$$a_{\pm}(z)=a_{\pm}\left[1+G_{\pm}(z)\left\{\left(\frac{a_{\pm}}{a'_{\pm}}\right)^2-1\right\}\right]^{-1/2}, \text{ where } G_{\pm}(z)=\frac{(2U_0^{\pm}-U_0^{\pm}g(z))U_0^{\pm}g(z)}{(U_0^{\pm})^2-m^2c^4} \tag{57}$$

This expression of waveguide cross-section (for the potential in Fig. 6(a)) implies that at $z<z_2$ and $z>z_1$ $G_{\pm}(z)=0$ and hence the cross-sections are $a_{\pm}(z)=a_{\pm}$ as depicted in the Fig. 6(b). At region II (i.e. $z_2<z<z_1$) $g(z)=1$ and hence $G_{\pm}(z)=\frac{1}{1-\left(mc^2/U_0^{\pm}\right)^2}$ leads to the minimum cross-sectional lengths inside the waveguide,

$$a_{\pm}^{min}=a_{\pm}\left[1+\left(\frac{1}{1-\left(mc^2/U_0^{\pm}\right)^2}\right)\left\{\left(\frac{a_{\pm}}{a'_{\pm}}\right)^2-1\right\}\right]^{-1/2}, \tag{58}$$

Therefore this waveguide corresponds to the scattering (due to this general step potential $U(z)$) of a spin less particle of incident wavelength $\lambda<2\times$ (least between $a_{\pm}^{min}$).

Now in our case of Hulthen potential $V(z)$ (Eq. 1) the cross-sectional distribution of the analogous waveguide simply can be understood from Eq. 57. The function $G(z)$ for

the general step potential is now replaced by $H(z)$ such that $V^{\pm}(z) = V_0^{\pm} H^{\pm}(z)$, where $V_0^{\pm}$ are the peaks of the potential $V(z)$ for $z \to 0^{\pm}$ respectively. For the Hulthen potential $V^{\pm}(z)$ are written as,

$$\begin{aligned} V^{+}(z) &= \frac{V_2}{e^{\alpha_2 z} - Q_2} = V_0^{+} \left(\frac{1 - Q_2}{e^{\alpha_2 z} - Q_2} \right) \equiv V_0^{+} h^{+}(z), \quad \text{where} \quad V_0^{+} = \frac{V_2}{1 - Q_2} \; ; \\ V^{-}(z) &= \frac{V_1}{e^{-\alpha_1 z} - Q_1} = V_0^{-} \left(\frac{1 - Q_1}{e^{-\alpha_1 z} - Q_1} \right) \equiv V_0^{-} h^{-}(z), \quad \text{where} \quad V_0^{-} = \frac{V_1}{1 - Q_1} \; . \end{aligned} \tag{59}$$

For the complex Hulthen potential $V(z)$ with the parameters given in Eq. 3 we consider a system of two single-mode waveguides coupled [45, 46] to each other corresponding to the real and imaginary part of $V(z)$. We denote the two waveguides as WG^R and WG^I which are corresponding to the real and the imaginary parts of $V(z)$ respectively. For a non-zero coupling between WG^R and WG^I the system mimics the quantum mechanical scattering through a non-Hermitian Hulthen potential. The cross-sectional distributions (analogous to Eq. 57) for the waveguides WG^R and WG^I are given as,

$$\begin{aligned} A_{\pm}^{R}(z) &= A_{\pm}^{R} \left[1 + Re[H_{\pm}(z)] \left\{ \left(\frac{A_{\pm}^{R}}{A_{\pm}^{\prime R}} \right)^2 - 1 \right\} \right]^{-1/2} , \\ A_{\pm}^{I}(z) &= A_{\pm}^{I} \left[1 + Im[H_{\pm}(z)] \left\{ \left(\frac{A_{\pm}^{I}}{A_{\pm}^{\prime I}} \right)^2 - 1 \right\} \right]^{-1/2} \end{aligned} \tag{60}$$

where

$$H^{\pm}(z) = \frac{(2V_0^{\pm} - V_0^{\pm} h^{\pm}(z)) V_0^{\pm} h^{\pm}(z)}{(V_0^{\pm})^2 - m^2 c^4} \tag{61}$$

$A_{\pm}^{R}$ and $A_{\pm}^{I}$ are the cross-sectional lengths of the WG^R and WG^I respectively when $Re[H_{\pm}(z)] = 0$ and $Im[H_{\pm}(z)] = 0$, i.e. at the region where $V^{\pm}(z) = 0$. $A_{\pm}^{\prime R}$ and $A_{\pm}^{\prime I}$ are the cross-sectional lengths of the waveguides WG^R and WG^I respectively at $z \to 0^{\pm}$ which actually correspond to the peaks (i.e. $V_0^{\pm}$) of the potential $V(z)$. Relation between $A_{\pm}^{\prime R}$, $A_{\pm}^{\prime R}$ and $A_{\pm}^{\prime I}$, $A_{\pm}^{\prime I}$ (assuming $Re[V_0^{-}] > Re[V_0^{+}]$ and $Im[V_0^{-}] > Im[V_0^{+}]$) are written as in Eq. 55,

$$\begin{aligned} A_{+}^{\prime R} &= A_{-}^{\prime R} + 2 \left(Re[V_0^{-}] - Re[V_0^{+}] \right) \text{ with } A_{-}^{\prime R} > 0, \\ A_{+}^{\prime I} &= A_{-}^{\prime I} + 2 \left(Im[V_0^{-}] - Im[V_0^{+}] \right) \text{ with } A_{-}^{\prime I} > 0. \end{aligned} \tag{62}$$

From Eq. 59 we see that $h^{\pm}(z) = 1$ for $z \to 0^{\pm}$, thus the minimum cross-sectional lengths of WG^R and WG^I are written from Eqs. 60 and 61 as,

$$\begin{aligned} A^{R}{}_{\pm}^{min} &= A_{\pm}^{R} \left[1 + \left(\frac{1}{1 - \left(mc^2 / Re[V_0^{\pm}] \right)^2} \right) \left\{ \left(\frac{A_{\pm}^{R}}{A_{\pm}^{\prime R}} \right)^2 - 1 \right\} \right]^{-1/2} , \\ A^{I}{}_{\pm}^{min} &= A^{I} \pm \left[1 + \left(\frac{1}{1 - \left(mc^2 / Im[V_0^{\pm}] \right)^2} \right) \left\{ \left(\frac{A_{\pm}^{I}}{A_{\pm}^{\prime I}} \right)^2 - 1 \right\} \right]^{-1/2} \end{aligned} \tag{63}$$

The electromagnetic wave propagating through the system of coupled waveguide experience both elastic scattering (due to WG^R) and inelastic scattering (due to WG^I). This coupled waveguide describes the scattering of a spin less particle due to non-Hermitian Hulthen potential if the wavelength of the incoming wave is smaller than the two times of the least cross-sectional lengths among the values of $A_{\pm}^{R^{min}}$ and $A_{\pm}^{I^{min}}$. By taking the cross-sectional lengths of the two ends of waveguides WG^R and WG^I as $A_{\pm}^{R} = A_{-}^{\prime R} + 2Re[V_0^-]$ and $A_{\pm}^{I} = A_{-}^{\prime I} + 2Im[V_0^-]$ respectively we present the geometrical views of WG^R and WG^I in Fig. 7 (b, d) corresponding to the parameters of the real and imaginary parts of the potential in Fig. 7(a, c) which leads to broadband CPA. The four cross-sectional lengths inside the waveguides in Fig. 7 (b, d) are calculated from Eq. 63 as $A_{+}^{R^{min}} = 197.026\ nm$ and $A_{-}^{R^{min}} = 197\ nm = A_{-}^{I^{min}}$ and $A_{+}^{I^{min}} = 197.01\ nm$. Therefore for these two coupled waveguides in Fig 7(b, d) the operating wavelength of the incoming wave must be smaller than two times of $A_{-}^{R^{min}}$ i.e. $\lambda_{max} \approx 394\ nm$. Similar waveguides with different physical dimension can also be constructed for different parametric regions of the non-Hermitian Hulthen potential which leads to broadband CPA.

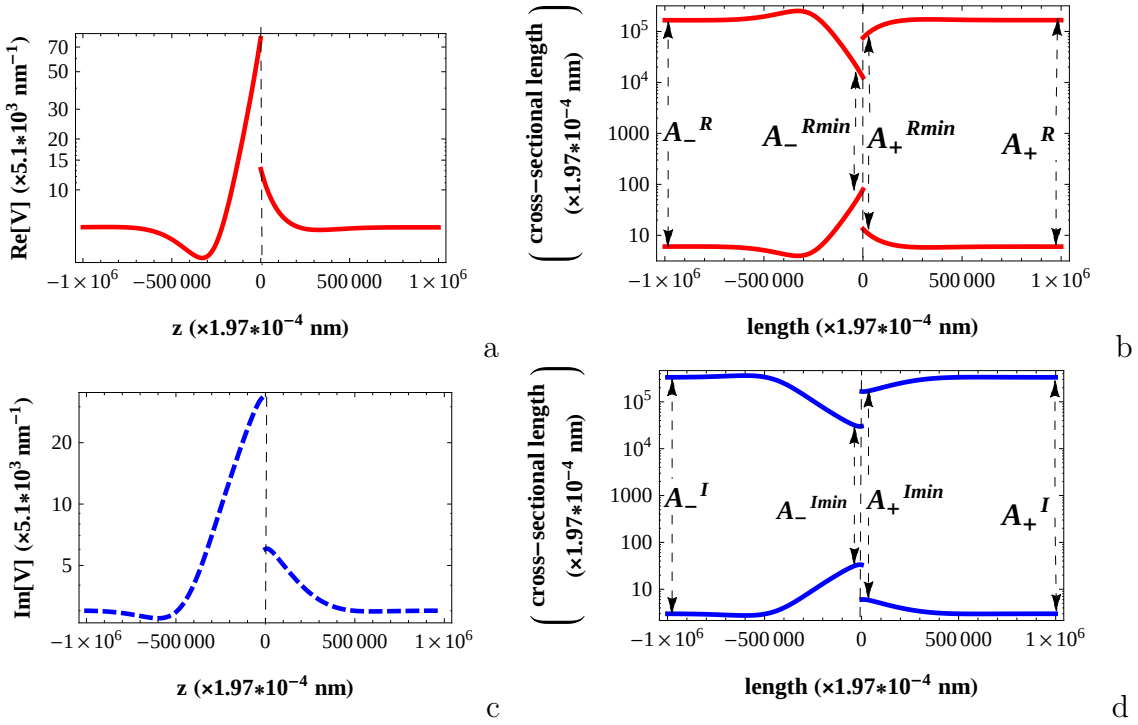

Fig. 7: Real and imaginary parts of a non-Hermitian Hulthen potential is plotted in 7(a) and 7(c) respectively with the parameters $q_1 = q_2 = 0.4, v_1 = 2.53 \times 10^5\ nm^{-1}, v_2 = 2.53 \times 10^4\ nm^{-1}, a_1 = a_2 = .051\ nm^{-1}, \phi_1 = \phi_2 = 0.3, \gamma_1 = \gamma_2 = 2.5, \beta_1 = \beta_2 = 0.2,$. The cross-sectional lengths and dimension of the corresponding waveguides are shown in 7(b) and 7(d).

4 Conclusions and Discussions

Null scattering (CC, CPA) and super-scattering (lasing), two extreme scattering situations are important tools in characterizing scattering due to complex potentials. In particular the occurrence of total absorption through a complex potential becomes very exciting due to the recent discovery of anti-laser which has number of technological applications. The occurrence of CPA and CC has so far been shown only for certain discrete values of the incidence energies of the particle and that too only for certain specific potentials. In a recent work we were able to show CPA for certain small ranges of incidence energies for well known nuclear potential [38]. In this work we parametrize the well known Hulthen potential in such a manner that it shows both unidirectional and bidirectional perfect absorption almost for the entire range of incidence energy. We have arrived to our conclusion analytically as well as graphically by considering both unidirectional and bidirectional incidence of the particles. The low energy scattering behavior of this potential is different from that of at high energies. We have shown that further fine tuning is required within the ranges of the parameters to achieve CPA for the low energy scattering. We would like to emphasize that over this entire range of incident energy the values of reflectance (R) and transmittance (T) are very very small ($\sim 10^{-24}$ or less). We call this potential as a 'black potential' which leads to broadband CPA. The values of R and T become less and less as we go on increasing incident energy. To classically design and to test our results one needs to know the waveguide analogy of this particular potential. We have provided the cross-sectional views of the waveguides analogous to our complex potential. Physical dimensions like lengths and cross-sectional lengths of the waveguides corresponding to real and imaginary parts of the non-Hermitian Hulthen potential are demonstrated graphically and the operating wavelength ($\lambda_{max} \approx 394\ nm$) of the coupled waveguides is analytically calculated.

Acknowledgment: BPM acknowledges the financial support from the Department of Science & Technology (DST), Govt. of India, under SERC project sanction grant No. SR/S2/HEP-0009/2012 and MH is thankful to Dr. S. K. Shivakumar, Director, ISAC for his support to carry out this research work. AG acknowledges the Council of Scientific & Indus- trial Research (CSIR), India for Senior Research Fellowship.

A Appendix: Relativistic Scattering coefficients of Hulthen potential

The general solutions of KG equation (by adopting natural units with $m = \hbar = c = 1$) for the Hulthen potential at $z < 0$ (i.e. $V^-(z) = \frac{V_1}{e^{-\alpha_1 z} - Q_1}$) are in terms of hyper-geometric function as follows,

$$\begin{aligned}\phi_L(z) &= (1 - Q_1 e^{\alpha_1 z})^{\lambda_1} \Big\{ A (Q_1 e^{\alpha_1 z})^{\mu_1} F(\mu_1 - \nu_1 + \lambda_1, \mu_1 - \nu_1 + \lambda_1, 1 + 2\mu_1; Q_1 e^{\alpha_1 z}) \\ &+ B (Q_1 e^{\alpha_1 z})^{-\mu_1} F(-\mu_1 - \nu_1 + \lambda_1, -\mu_1 + \nu_1 + \lambda_1, 1 - 2\mu_1; Q_1 e^{\alpha_1 z}) \Big\} \qquad (64)\end{aligned}$$

Similarly the solutions for $V^+(z) = \frac{V_2}{e^{\alpha_2 z} - Q_2}$ (at $z > 0$) are,

$$\begin{aligned}\phi_R(z) &= (1 - Q_2 e^{-\alpha_2 z})^{\lambda_2} \Big\{ C (Q_2 e^{-\alpha_2 z})^{\mu_2} F(\mu_2 - \nu_2 + \lambda_2, \mu_2 - \nu_2 + \lambda_2, 1 + 2\mu_2; Q_2 e^{-\alpha_2 z}) \\ &+ H (Q e^{-\alpha z})^{-\mu_2} F(-\mu_2 - \nu_2 + \lambda_2, -\mu_2 + \nu_2 + \lambda_2, 1 - 2\mu_2; Q_2 e^{-\alpha_2 z}) \qquad (65)\end{aligned}$$

where the following notations are used,

$$\mu_1 = ik/\alpha_1;\ \mu_2 = ik/\alpha_2;\ k = \sqrt{E^2 - 1} \qquad (66)$$

$$\lambda_1 = 1/2 + 1/2\sqrt{1 - \Big(\frac{2V_1}{\alpha_1 Q_1}\Big)^2}\ ; \lambda_2 = 1/2 + 1/2\sqrt{1 - \Big(\frac{2V_2}{\alpha_2 Q_2}\Big)^2} \qquad (67)$$

$$\nu_1 = \sqrt{\mu_1^2 + \lambda_1^2 - \lambda_1 - \frac{2EV_1}{\alpha_1^2 Q_1}};\ \nu_2 = \sqrt{\mu_2^2 + \lambda_2^2 - \lambda_2 - \frac{2EV_2}{\alpha_2^2 Q_2}} \qquad (68)$$

The asymptotic form of ϕ_L and ϕ_R are given as,

$$\begin{aligned}\phi_L(z \to -\infty) &\to A Q_1^{ik/\alpha_1} e^{ikz} + B Q_1^{-ik/\alpha_1} e^{-ikz}\ ; \\ \phi_R(z \to +\infty) &\to C Q_2^{ik/\alpha_2} e^{-ikz} + H Q_2^{-ik/\alpha_2} e^{ikz} \qquad (69)\end{aligned}$$

Using Eq. 69 the left and right handed scattering amplitudes are calculated as,

$$r_l = B/A = \frac{Q_1^{2\mu_1}\Big[- F_1 F_2 (N_1 + N_2) + c_1 F_1^{'} F_2 + c_3 F_2^{'} F_1\Big]}{D} \equiv Q_1^{2\mu_1} \tilde{F_{rl}} \qquad (70)$$

$$t_l = H/A = \frac{Q_1^{2\mu_1}\Big[2M F_1 F_4 + c_1 F_1^{'} F_4 - c_2 F_4^{'} F_1\Big]}{D} \Big(\frac{1}{u}\Big) \equiv \frac{Q_1^{2\mu_1}}{u} \tilde{F_{tl}} \qquad (71)$$

$$r_r = H/C = \frac{Q_2^{2\mu_2}\Big[- F_3 F_4 (N_1 + N_2) + c_4 F_3^{'} F_4 + c_2 F_4^{'} F_3\Big]}{D} \equiv Q_2^{2\mu_2} \tilde{F_{rr}} \qquad (72)$$

$$t_r = B/C = \frac{Q_2^{2\mu_2}\Big[2M F_3 F_2 + c_4 F_3^{'} F_2 - c_3 F_2^{'} F_3\Big] u}{D} \equiv Q_2^{2\mu_2} u \tilde{F_{tr}} \qquad (73)$$

where

$$D = 2MF_4F_2 + F_4F_2(N_1+N_2) - c_2F_4^{'}F_2 - c_3F_2^{'}F_4 \ \ \text{with} M = ik \ ; \tag{74}$$

with

$$N_1 = \frac{Q_1\alpha_1\lambda_1}{1-Q_1} \ ; \ N_2 = \frac{Q_2\alpha_2\lambda_2}{1-Q_2} \ ; \tag{75}$$

$$u = \frac{Q_2^{-\mu_2}(1-Q_2)^{\lambda_2}}{Q_1^{-\mu_1}(1-Q_1)^{\lambda_1}} \tag{76}$$

$$\begin{aligned} c_1 &= \frac{(\mu_1+\lambda_1)^2-\nu_1^2}{1+2\mu_1}(Q_1\alpha_1) \ ; \ c_2 = \frac{(-\mu_1+\lambda_1)^2-\nu_1^2}{1-2\mu_1}(Q_1\alpha_1) \ ; \\ c_3 &= \frac{(-\mu_2+\lambda_2)^2-{\nu_2}^2}{1-2\mu_2}(Q_2\alpha_2) \ ; \ c_4 = \frac{(\mu_2+\lambda_2)^2-{\nu_2}^2}{1+2\mu_2}(Q_2\alpha_2) \ . \end{aligned} \tag{77}$$

The hyper-geometric functions are written as follows,

$$\begin{aligned} F_1 &= F(\mu_1-\nu_1+\lambda_1, \mu_1+\nu_1+\lambda_1, 1+2\mu_1; Q_1) \ ; \\ F_1^{'} &= F(\mu_1-\nu_1+\lambda_1+1, \mu_1+\nu_1+\lambda_1+1, 2+2\mu_1; Q_1) \ ; \end{aligned} \tag{78}$$

$$\begin{aligned} F_2 &= F(-\mu_2-\nu_2+\lambda_2, -\mu_2+\nu_2+\lambda_2, 1-2\mu_2; Q_2) \ ; \\ F_2^{'} &= F(-\mu_2-\nu_2+\lambda_2+1, -\mu_2+\nu_2+\lambda_2+1, 2-2\mu_2; Q_2) \end{aligned} \tag{79}$$

$$\begin{aligned} F_3 &= F(\mu_2-\nu_2+\lambda_2, \mu_2+\nu_2+\lambda_2, 1+2\mu_2; Q_2) \ ; \\ F_3^{'} &= F(\mu_2-\nu_2+\lambda_2+1, \mu_2+\nu_2+\lambda_2+1, 2+2\mu_2; Q_2) \ ; \end{aligned} \tag{80}$$

$$\begin{aligned} F_4 &= F(-\mu_1-\nu_1+\lambda_1, -\mu_1+\nu_1+\lambda_1, 1-2\mu_1; Q_1) \ ; \\ F_4^{'} &= F(-\mu_1-\nu_1+\lambda_1+1, -\mu_1+\nu_1+\lambda_1+1, 2-2\mu_1; Q_1); \end{aligned} \tag{81}$$

References

[1] C. M. Bender and S. Boettcher, *Phys. Rev. Lett.* **80**, 5243 (1998).

[2] A. Mostafazadeh, *Int. J. Geom. Meth. Mod. Phys.* **7**, 1191(2010) and references therein.

[3] C.M. Bender, *Rep. Progr. Phys.* **70** (2007) 947 and references therein.

[4] Z. H. Musslimani, K. G. Makris, R. El-Ganainy, and D. N. Christodoulides, *Phys. Rev. Lett.* **100**, 030402 (2008).

[5] C. E. Ruter, K. G. Makris, R. El-Ganainy, D. N. Christodoulides, M. Segev, D. Kip, *Nature Phys.* **6** 192, (2010);

[6] R. El-Ganainy, K. G. Makris, D. N. Christodoulides and Z. H. Musslimani, *Opt. Lett.* **32**, 2632 (2007).

[7] A. Guo et al, *Phys. Rev. Lett.* **103**, 093902 (2009).

[8] A. Ghatak and B. P. Mandal, *J. Phys. A: Math. Theor.* **45**, 355301 (2012).

[9] B. P. Mandal and S S. Mahajan *arXiv:1312.0757*, (2013).

[10] B. P. Mandal, B. K. Mourya, and R. K. Yadav (BHU), *Phys. Lett. A* **377**, 1043 (2013).

[11] B. P. Mandal, *Mod. Phys. Lett. A* **20**, 655(2005).

[12] B. P. Mandal and A. Ghatak, *J. Phys. A: Math. Theor.* **45**, 444022 (2012) .

[13] T. Kato, *Perturbation Theroy of Linear Operators*, **Springer**, Berlin, (1966).

[14] M. V. Berry, *Czech. J. Phys.* **54**, 1039 (2004).

[15] W. D. Heiss, *Phys. Rep.* **242**, 443 (1994).

[16] A. Mostafazadeh, *Phys. Rev. Lett.* **102**, 220402 (2009).

[17] A. Mostafazadeh, M. Sarisaman, *Phys. Lett. A* **375**, 3387 (2011).

[18] A. Ghatak, R. D. Ray Mandal, B. P. Mandal, *Ann. of Phys.* **336**, 540 (2013).

[19] A. Ghatak, J. A. Nathan, B. P. Mandal, and Z. Ahmed, *J. Phys. A: Math. Theor.* **45**, 465305 (2012).

[20] S. Longhi, *J. Phys. A: Math. Theor.* **44**, 485302 (2011).

[21] A. Mostafazadeh, *Phys. Rev. A* **87**, 012103 (2013).

[22] L. Deak, T. Fulop, *Ann. of Phys.* **327**, 1050 (2012).

[23] C. F. Gmachl, *Nature* **467**, 37 (2010).

[24] S. Longhi, *Physics* **3**, 61(2010).

[25] W. Wan, Y. Chong, L. Ge, H. Noh, A. D. Stone, H. Cao, *Science* **331**, 889 (2011).

[26] N. Liu, M. Mesch, T. Weiss, M. Hentschel, and H. Giessen, *Nano Lett.* **10**, 2342 (2010).

[27] H. Noh, Y. Chong, A. Douglas Stone, and Hui Cao, *Phys. Rev. Lett.* **108**, 6805 (2011).

[28] A. Mostafazadeh and M. Sarisaman, *Proc. R. Soc. A* **468**, 3224 (2012).

[29] S. Longhi, *Phys. Rev. A* **83**, 055804 (2011).

[30] S. Dutta-Gupta, R. Deshmukh, A. Venu Gopal, O. J. F. Martin, and S. Dutta Gupta, *Opt. Lett.* **37**, 4452 (2012).

[31] N. Liu, M. Mesch, T. Weiss, M. Hentschel, and H. Giessen, *Nano Lett.* **10** 2342 (2010).

[32] M. Cai, O. Painter, and K. J. Vahala, *Phys. Rev. Lett.* **85**, 74 (2000).

[33] J. R. Tischler, M. S. Bradley, and V. Bulovic, *Opt. Lett.* **31**, 2045 (2006)

[34] S. Dutta Gupta, *Opt. Lett.* **32**, 1483 (2007).

[35] S. Balci, C. Kocabas, and A. Aydinli, *Opt. Lett.* **36**, 2770 (2011).

[36] S. Balci, Er. Karademir, C. Kocabas, and A. Aydinli, *Opt. Lett.* **36**, 3041 (2011).

[37] A. Mostafazadeh, *J. Phys. A: Math. Theor.* **45**, 444024 (2012).

[38] M. Hasan, A. Ghatak, B. P. Mandal, *Ann. of Phys.* **344** , 17 (2014).

[39] J. Guo, X. Fang, *Can. J. Phys.*, **87** 1021 (2009).

[40] Pham Loi Vu, *Acta App. Math.*, **49** 107 (1997).

[41] M S Marinov and B. Segev, *J. Phys. A: Math. Gen.* **29** 2839 (1996).

[42] I. S. Gradshteyn, I. M. Ryzhik, A. Jaffrey *'Table of Integrals, Series and Products'*, *Academic press* (1965).

[43] L. I. Schiff, *'Quantum Mechanics'*, *McGraw-Hill international edition* (1968).

[44] M. Campi, *Am. J. Phys.*, **35**, 133 (1967).

[45] A. Paul, A. Saha, S. Bandopadhyay, and B. Dutta-Roy, *Eur. Phys. J. D* **42**, 495 (2007).

[46] G. S. Agarwal and K. Qu, *Phys. Rev. A* **85**, 031802 (R) (2012).